Available online at www.sciencedirect.com
SCIENCE DIRECT®
Journal of Magnetic Resonance 174 (2005) 301–309
JMR Journal of Magnetic Resonance
www.elsevier.com/locate/jmr

Correlating fast and slow chemical shift spinning sideband patterns in solid-state NMR

Robin M. Orr [a], Melinda J. Duer [a,*], Sharon E. Ashbrook [b]

[a] Department of Chemistry, University of Cambridge, Lensfield Road, Cambridge CB2 1EW, UK
[b] Department of Earth Sciences, University of Cambridge, Downing Street, Cambridge CB2 3EQ, UK

Received 22 November 2004; revised 18 February 2005
Available online 25 March 2005

Abstract

An experiment is presented that enables the measurement of small chemical shift anisotropy tensors under fast magic-angle spinning (MAS). The two-dimensional spectra obtained give a fast MAS sideband pattern in the directly observed dimension with the spinning sideband intensities equivalent to the chemical shift anisotropy scaled by a factor of N, or equivalently the sample spinning frequency scaled by $1/N$, in the indirectly observed dimension. The scaling factor may be arbitrarily varied by changing the number and timings of the rotor synchronized π-pulses used. Desirable features of the experiment include a fixed length pulse sequence and efficient sampling of the indirectly observed dimension. In addition, neither quadrature detection in the indirect dimension nor storage periods are required, consequently no signal intensity is discarded by the pulse sequence. The experiment is demonstrated using ^{31}P NMR of sodium phosphate and ^{13}C NMR of fumaric acid monoethyl ester for which a scaling factor of $N = 10.2$ was employed.

Keywords: Solid-state NMR; Magic-angle spinning; Chemical shift anisotropy; Recoupling

1. Introduction

The measurement of chemical shift principal tensor values has, for many years, been an established technique for investigating molecular structure and dynamics in the field of solid-state NMR. If the effects of other nuclear spin interactions are absent, or negligible, the singularities in broad powder-pattern lineshapes observed in the spectra of static powder samples can be used to determine the chemical shift principal tensor values. For most samples, however, the overlap of powder patterns from several chemical sites hinders the extraction of this information.

Magic-angle spinning (MAS) of the sample improves the resolution of solid-state NMR spectra. If the spinning frequency is of the order of the chemical shift anisotropy (CSA), or less, spinning sidebands spaced at the sample spinning frequency and centred about the isotropic shift are observed in the spectrum. The intensities of these spinning sidebands may be used to determine chemical shift principal tensor values [1,2]. For accurate results to be achieved, it is necessary that many spinning sidebands are present in the spectrum: about five significant spinning sidebands are needed to determine the anisotropy (for asymmetry parameters in the range $0.1 < \eta < 1$), whilst 6–10 sidebands are required to determine the asymmetry ($0.3 < \eta < 1$) [3]. The assignment of numerous spinning sidebands in the complex spectra of large molecules, with many different chemical sites can complicate this sideband analysis. Alternative methods are based on two-dimensional experiments in which the chemical shift anisotropy is recoupled in some form in one dimension of the experiment, whilst isotropic signals are retained in the other to provide the necessary resolution. One approach is to

* Corresponding author. Fax: +44 1223 336362.
E-mail address: mjd13@cam.ac.uk (M.J. Duer).

1090-7807/$ - see front matter © 2005 Elsevier Inc. All rights reserved.
doi:10.1016/j.jmr.2005.03.001

recouple chemical shift under MAS to obtain quasi-static (scaled) powder patterns in the indirect dimension separated by isotropic shifts in the directly observed dimension, from which chemical shift parameters may be simply read off the powder patterns under favourable circumstances. Some of these experiments can often be technically demanding, such as magic-angle-turning [4] and variable-angle correlation [5]. However, a range of such experiments exist which are relatively straightforward to implement and can give good results. The first such method, due to Tycko et al. [6] is sensitive to pulse imperfections and so has been modified by Schmidt-Rohr and co-workers [7] in the SUPER experiment. Both experiments have been utilized with good results, although because of the large scaling of the chemical shift anisotropy induced by the latter experiment, the range of spinning frequencies under which it may be used is relatively restricted.

Despite these developments, one fundamental problem remains: the chemical shift anisotropy information is spread out over a broad powder pattern and so signal-to-noise is a very real issue, especially when dealing with small samples, as is becoming increasingly common with the uptake of solid-state NMR methodology by biologists. In such cases, a far better approach is to distil the chemical shift anisotropy information into discrete sidebands. This is the approach of the 2D-PASS experiment by Antzutkin et al. [8].

However, if the CSA is small, the need to measure the intensities of several spinning sidebands introduces two problems; the slow sample spinning frequency necessary to observe sufficient numbers of spinning sidebands is difficult to stabilize, and homonuclear dipolar interactions affect the sideband intensities to a greater extent at slow spinning rates. This has led to interest in developing 2D experiments that correlate an isotropic spectrum in one dimension with sideband intensities similar to those obtained if the CSA were a factor of N larger, or equivalently the sample spinning rate reduced by a factor of $1/N$, in the other dimension [9–14]. These experiments can be grouped into those that give identical sideband intensities to those obtained in the MAS spectra at the effective spinning rate (ω_r/N), and experiments where intensities are altered.

This latter group has the disadvantage of requiring non-conventional data analysis to determine the CSA parameters. Falling in this group, one of the earliest experiments that achieves the above aim is the spin-echo experiment of Kolbert et al. [9]. A scaling factor of N is accomplished using $(N-1)$ π-pulses spaced uniformly throughout the incremented t_1 period. While the simplicity and comparatively few pulses required favour this method, the more complex data analysis is undesirable. The same processing problem arises in the recently reported ROSES experiment [13]. The indirectly observed dimension is sampled at intervals of $\tau_r + \tau$; between these times a delay τ, which determines the scaling factor, is followed by a pair of π-pulses separated by half a rotor period. The isotropic shift is scaled, but not suppressed, in the ω_1 dimension; thus extensive sampling of this dimension is required to achieve sufficient resolution. For long t_1 periods, the number of π-pulses becomes large, and spectrometer and spinning stability is likely to become important. However, very large scaling factors (up to $N = 30$) have been demonstrated using ROSES.

There are three experiments which give sidebands intensities identical to the usual MAS spectra that would be obtained at the scaled spinning frequency, and allow determination of chemical shift tensor values by the usual, well established, methods [1,2]. The extended chemical-shift modulation (XCS) experiment has a constant length pulse sequence of N rotor periods during which $(2N-1)$ π-pulses are applied [10]. $(N-1)$ of the π-pulses are fixed at the end of even rotor periods; the remaining π-pulses are also separated by two rotor periods, but their timing relative to the other pulses is incremented during the experiment. Although the sequence allows evolution of the magnetization due to the isotropic chemical shift in the indirectly observed dimension, by combining two spectra and transforming as specified by Gullion [10], the isotropic shift is removed from this dimension. This leads to favourably efficient sampling of the indirect dimension, as the number of t_1 increments is only twice the maximum order of spinning sideband to be measured. The SPEED MAS experiment of Strohmeier and Grant uses essentially the same pulse sequence as XCS [14]. Implemented as they propose, it does not eliminate the isotropic shift in the ω_1 dimension. Consequently, many t_1 increments are need, although reconstruction of the signal in the indirectly observed dimension using replication was demonstrated to reduce the number of increments necessary to achieve good resolution.

In the CSA amplification method, two identical units of four, five or seven π-pulses are applied over an integer number of rotor periods [11,12]. These are separated by a period during which the transverse magnetization is stored along the z-axis of the rotating frame for a period t_1 that is varied throughout the two-dimensional experiment. This method is a modification of the experiment of De Lacroix et al. [15] and is related to the 2D-PASS experiment [8]. Isotropic shifts in the ω_1 dimension do not occur; thus, as with the XCS experiment, a minimal number of t_1 increments are required. Scaling factors up to $N = 12$ have been demonstrated experimentally. The CSA amplification method and the XCS method would thus appear to be the experiments of choice when facing the scenario of measuring small chemical shift anisotropies. Their only potential drawback is the need for two spectra in the case of the XCS experiment and a storage period for the magnetization in the CSA amplification

experiment, which halves the final signal intensity. Thus both experiments potentially suffer from sensitivity issues not encountered in experiments where the chemical shift anisotropy is not amplified. The ideal experiment would be one in which the chemical shift anisotropy could be amplified but signal not lost relative to an unamplified chemical shift anisotropy determination experiment. Here, we present a new experiment which works towards that goal. This experiment is in essence a combination of the 2D-PASS [8] and Titman and coworkers' CSA amplification method [11,12].

The pulse sequence for the new experiment, which we refer to for convenience as 2D CSA-amplified PASS, is illustrated in Fig. 1A. Transverse magnetization is generated by cross-polarization [16], which is appropriate for ^{13}C NMR of organic solids. During the 2D experiment the evolution period in the indirect dimension has a fixed duration, however the timing of the rotor synchronized π-pulses changes. Each slice of the experiment is associated with a value of the variable Θ, which is linearly incremented in a convenient number of steps between 0 and 2π as the 2D spectrum is recorded. Each value of Θ corresponds to a unique set of π-pulse times that would be used for recording a slice of the 2D experiment associated with this value. The π-pulse times as a function of Θ are plotted for scaling factors $N = 3$ and $N = 2$ in Fig. 1, where the evolution time is four rotor periods. A sequence without storage periods, different to that proposed here, was first suggested by Crockford [17], although experimental results were not presented. We note that 2D CSA-amplified PASS has a number of favourable features; first, a gain in signal intensity by a factor of 2 is achieved over experiments that require either a storage period or where quadrature detection in the indirect dimension is required. Second, in common with the XCS and CSA amplification experiments, isotropic shifts do not occur in the ω_1 dimension, leading to efficient sampling of the indirect dimension. Finally, spinning sideband intensities are the same as in conventional MAS spectra allowing routine analysis.

2. Theory

The orientation of the CSA principal axis frame with respect to the rotor frame of reference is defined by the Euler angles $\{\alpha, \beta, \gamma\}$. It is convenient to use the idea of "carousels' of crystallites, introduced by Levitt [19], that have common Euler angles α and β. The rotating frame precession frequency of each crystallite in a MAS sample is periodic with the rotor period and Fourier expansion of this precession frequency may be made:

$$\omega_c(t;\gamma) = \sum_m \omega_c^{(m)}(\gamma)\exp(im\omega_r t), \tag{1}$$

where the subscript index c indicates the carousel and ω_r is the spinning frequency ($\omega_r = 2\pi/\tau_r$). For the chemical shielding interaction it may be shown that the sum over m is limited to the range $-2 \leqslant m \leqslant 2$ and that for a sample spinning at the magic-angle ($\tan^{-1}\sqrt{2}$) the Fourier coefficient $\omega_c^{(0)}$ is independent of γ and equal to the isotropic shift [20,21]. In addition, since any crystallite within a carousel can be brought into the orientation of another by rotation of the sample about the rotor axis, the Fourier components obey the relation

$$\omega_c^{(m)}(\gamma) = \omega_c^{(m)}(0)\exp(im\gamma). \tag{2}$$

We follow the formalism and notation presented by Antzutkin et al. [8] in their development of the 2D-PASS experiment. The time coordinate is chosen such that $t = 0$ coincides with the start of signal detection, and the pulse sequence starts with transverse magnetization at time $t = -T$. In the ideal case, this is followed by a sequence of n infinitely strong π-pulses given the index q, $q = 1, 2, \ldots, n$, at times $t = -T + \tau_q$. The five pulse case is illustrated in Fig. 1A. The phase of the magnetization

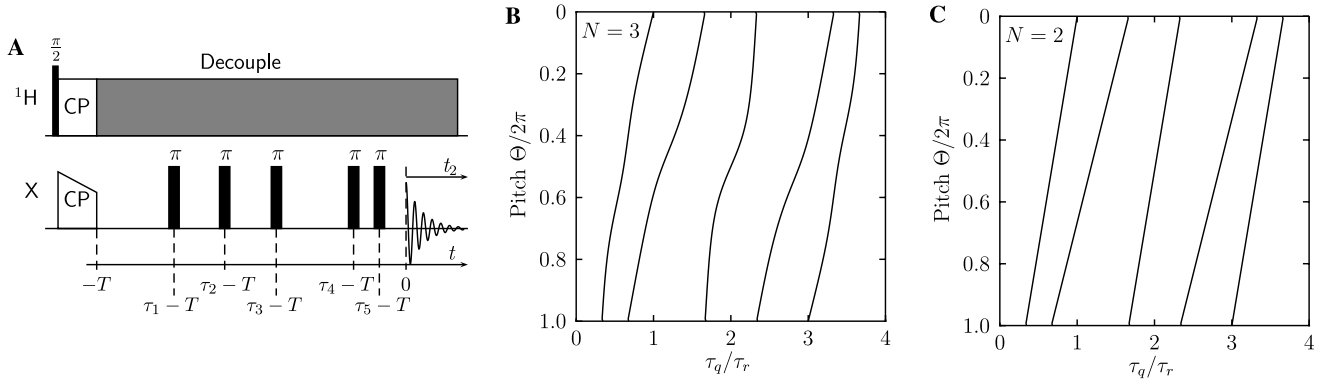

Fig. 1. (A) The five pulse 2D CSA-amplified PASS sequence for scaling factors of $N \leqslant 3$. The sequence is illustrated with the initial transverse magnetization generated using ramped cross-polarization (CP) [16,18]. During the 2D experiment, the pseudo t_1 variable Θ is incremented between 0 and 2π; the π-pulse timings required for each value of Θ are illustrated in the plots below the pulse sequence for $N = 3$ (B), and $N = 2$ (C), where each line plots the timing of one pulse as a function of Θ.

of an individual crystallite at the start of signal detection, assuming an initial phase of zero at $t = -T$, is given by

$$\phi_c(0;\gamma) = \Phi_c(0, -T+\tau_n;\gamma) - \Phi_c(-T+\tau_n, -T+\tau_{n-1};\gamma) \cdots + (-1)^n \Phi_c(-T+\tau_1, -T;\gamma) \quad (3)$$

with the function Φ_c defined as

$$\Phi_c(t_b, t_a;\gamma) = \int_{t_a}^{t_b} \omega_c(t;\gamma)\,dt, \quad (4)$$

$$= \omega_c^{(0)}(t_b - t_a) + \xi_c(t_b;\gamma) - \xi_c(t_a;\gamma), \quad (5)$$

$$\xi_c(t;\gamma) = \sum_{m\neq 0} \frac{\omega_c^{(m)}(\gamma)\exp(im\omega_r t)}{im\omega_r}. \quad (6)$$

This gives the phase of the magnetization at the start of signal acquisition to be

$$\phi_c(0;\gamma) = \omega_c^{(0)}\tau_{seq} + \xi_c(0;\gamma) - (-1)^n\left[2\sum_{q=1}^{n}(-1)^q \xi(-T+\tau_q;\gamma) + \xi_c(-T;\gamma)\right], \quad (7)$$

$$\tau_{seq} = T - 2\sum_{q=1}^{n}(-1)^{n+q}\tau_q. \quad (8)$$

In the directly observed dimension, the phase accumulation of the magnetization of a crystallite during the t_2 period is

$$\Phi_c(t_2;\gamma) = \omega_c^{(0)} t_2 + \xi_c(t_2;\gamma) - \xi_c(0;\gamma). \quad (9)$$

To achieve the desired scaling effect of the CSA by a factor of N in the indirect dimension, it is required that the evolution of the magnetization due to the anisotropic component of chemical shift is N times as rapid in the indirect dimension as in the directly observed dimension, whilst the isotropic shift is suppressed. Thus the phase of the magnetization of each individual crystallite at the start of signal detection must obey the condition

$$\phi_c(0,\gamma) = N\xi_c(0;\gamma) - N\xi_c\left(-\frac{\Theta}{\omega_r};\gamma\right), \quad (10)$$

$$\tau_{seq} = 0. \quad (11)$$

In this expression, $-\Theta/\omega_r$ is a pseudo t_1 variable that is incremented during the experiment. Θ is varied between 0 and 2π in a convenient number of steps, of the order of twice the desired number of sideband intensities. With this condition fulfilled the contribution of a crystallite to the detected signal is given by

$$s_c^{\Theta}(t_2,\gamma) = \exp i\left\{(N-1)\xi_c(0;\gamma) - N\xi_c\left(-\frac{\Theta}{\omega_r};\gamma\right) + \xi_c(t_2,\gamma) + \omega_c^{(0)}t_2\right\}\exp\{-\lambda(T+t_2)\}, \quad (12)$$

where λ describes the relaxation rate of the transverse magnetization.

Following the derivation for the signal intensity given in the description of the chemical shift amplification experiment [11,12], Fourier expansion of the terms in Eq. (12) involving $\xi_c(t;\gamma)$ may be made due to the periodicity of this function:

$$\exp\{i\xi_c(t;\gamma)\} = \sum_{k=-\infty}^{+\infty} C_c^{(k)}(\gamma)\exp(ik\omega_r t), \quad (13)$$

$$\exp\{iN\xi_c(t;\gamma)\} = \sum_{l=-\infty}^{+\infty} F_c^{(l)}(\gamma)\exp(il\omega_r t). \quad (14)$$

The Fourier coefficients in Eqs. (13) and (14) are defined respectively by

$$C_c^{(k)} = \frac{1}{2\pi}\int_0^{\tau_r}\exp\left\{\sum_{m\neq 0}\frac{\omega_c^{(m)}(\gamma)\exp(im\omega_r t)}{m\omega_r}\right\}\exp(-ik\omega_r t)\,dt, \quad (15)$$

$$F_c^{(k)} = \frac{1}{2\pi}\int_0^{\tau_r}\exp\left\{\sum_{m\neq 0}\frac{[N\omega_c^{(m)}(\gamma)]\exp(im\omega_r t)}{m\omega_r}\right\}\exp(-ik\omega_r t)\,dt, \quad (16)$$

$$= \frac{1}{2\pi}\int_0^{N\tau_r}\exp\left\{\sum_{m\neq 0}\frac{\omega_c^{(m)}(\gamma)\exp(i\frac{\omega_r}{N}mt')}{m\frac{\omega_r}{N}}\right\}\exp\left(-i\frac{\omega_r}{N}kt'\right)dt'. \quad (17)$$

Note that Eqs. (15) and (16) differ by only a scaling of the CSA by a factor of N. The change of variable between Eqs. (16) and (17), $t = t'/N$, highlights the equivalence of viewing this as a scaling of the sample spinning frequency by a factor of $1/N$. Eq. (12) is now re-expressed using these Fourier expansions:

$$s_c^{\Theta}(t_2,\gamma) = \sum_{l'}\sum_{k'}\sum_{l}\sum_{k} F_c^{(l')}(\gamma)[C_c^{(k')}(\gamma)]^*[F_c^{(l)}(\gamma)]^* \times C_c^{(k)}(\gamma)\exp\{i(\omega_c^{(0)} + k\omega_r)t_2\}\exp(il\Theta) \times \exp\{-\lambda(T+t_2)\}. \quad (18)$$

Substituting Eq. (2) into Eq. (18), and writing $C_c^{(k)}(0)$ as $C_c^{(k)}$:

$$s_c^{\Theta}(t_2,\gamma) = \sum_{l'}\sum_{k'}\sum_{l}\sum_{k} F_c^{(l')}[C_c^{(k')}]^*[F_c^{(l)}]^* C_c^{(k)} \times \exp\{i(\omega_c^{(0)} + k\omega_r)t_2\}\exp(il\Theta) \times \exp(i(k-k'+l'-l)\gamma)\exp\{-\lambda(T+t_2)\}. \quad (19)$$

If the sample is a finely divided powder, there is a continuous and uniform distribution of γ orientations within each carousel. The contribution to the measured NMR signal from a carousel is therefore the integral of Eq. (19) with respect to γ. Following this integration,

only the terms in the multiple summations with $k - k' + l' - l = 0$ remain:

$$s_c^{\Theta}(t_2) = \sum_{l'} \sum_{l} \sum_{k} F_c^{(l')} [C_c^{(k+l'-l)}]^* [F_c^{(l)}]^* C_c^{(k)} \times \exp\{i(\omega_c^{(0)} + k\omega_r)t_2\} \exp(il\Theta) \times \exp\{-\lambda(T + t_2)\}. \quad (20)$$

This initially predicts a complex 2D spectrum correlating the two fast and slow spinning sideband patterns, but if the spinning sidebands in the directly observed dimension are negligible, as may be the case if fast MAS is used, only $k = 0$ is significant in the sum. If this is not achieved, stroboscopic sampling at the spinning frequency can be made so that the the spinning sidebands are refocused at each point of signal detection and the summation over k is implicitly measured, giving the isotropic spectrum in the direct dimension. Alternatively the summation over k can be evaluated from the sideband correlation spectrum by adding the sideband intensities to that of the central peak of the direct dimension.

Eq. (20) corresponds to Eq. (15) in [12], and the summation over l' may be evaluated, as identified by Crockford and co-workers [11,12], using the property of the Fourier components:

$$\sum_{k=-\infty}^{+\infty} C_c^{(n+k)} [C_c^{(k)}]^* = \begin{cases} 1, & n = 0, \\ 0, & n \neq 0. \end{cases} \quad (21)$$

The resulting signal is then is described by

$$s_c^{\Theta}(t_2) = \sum_{l} F_c^{(l)} [F_c^{(l)}]^* \exp\{i\omega_c^{(0)} t_2\} \exp(il\Theta) \exp\{-\lambda(T + t_2)\}. \quad (22)$$

Following from Eqs. (15) and (16), the real quantity $F_c^{(l)}[F_c^{(l)}]^*$ is interpreted as the intensity of the lth spinning sideband due to the carousel c, with the CSA scaled by a factor of N. Averaging of Eq. (22) over all carousels, and 2D complex Fourier transform with respect to $-\Theta/\omega_r$ and t_2, demonstrates that the spectrum is represented by

$$S(\omega_1, \omega_2) = \exp(-\lambda T) \sum_{l=-\infty}^{+\infty} a^{(l)} \frac{\lambda}{\lambda + i(\omega_2 - \omega_{iso})} \delta(\omega_1 - l\omega_r), \quad (23)$$

where $a^{(l)}$ is the intensity of the lth spinning sideband with the scaled CSA. The spectrum has the required form, a peak at the isotropic shift in the directly observed dimension correlated with the spinning sideband intensities corresponding to the CSA scaled by a factor of N in the indirectly observed dimension. As stressed earlier, this can equally be represented as a scaling of the spinning frequency by $1/N$ by simply scaling the frequency axis in the indirect dimension by $1/N$. The constant pulse sequence length ensures that the relaxation in the effective t_1 dimension simply scales the intensity of the whole spectrum by $\exp(-\lambda T)$ and the relative sideband intensities are of the same form as in the 1D MAS spectrum at the effective spinning frequency of ω_r/N.

3. Calculation of pulse sequences

Defining the quantities $\Theta_q = \tau_q \omega_r$ and $\Theta_T = T\omega_r$ [8], from Eq. (10), the pulse sequence for the period $-T \leqslant t \leqslant 0$ must fulfil the following condition, for all crystallite orientations:

$$0 = (-1)^n \left[2 \sum_{q=1}^{n} (-1)^q \sum_{m \neq 0} \frac{\omega_c^{(m)}(\gamma) e^{(im(\Theta_q - \Theta_T))}}{im\omega_r} + \sum_{m \neq 0} \frac{\omega_c^{(m)}(\gamma) e^{(-im\Theta_T)}}{im\omega_r} \right] + (N-1) \sum_{m \neq 0} \frac{\omega_c^{(m)}(\gamma)}{im\omega_r} - N \sum_{m \neq 0} \frac{\omega_c^{(m)}(\gamma) e^{(-im\Theta)}}{im\omega_r}. \quad (24)$$

By equating terms with equal coefficients in $\omega_c^{(m)}(\gamma)/(im\omega_r)$, we obtain

$$0 = (N-1) e^{(im\Theta_T)} - N e^{\{im(\Theta_T - \Theta)\}} + (-1)^n \left[2 \sum_{q=1}^{n} (-1)^q e^{(im\Theta_q)} + 1 \right] \quad (25)$$

for $m = 1$ and $m = 2$. To prevent phase accumulation due to the isotropic shift, a further condition, Eq. (11), must also be satisfied:

$$\Theta_T - 2 \sum_{q=1}^{n} (-1)^{n+q} \Theta_q = 0. \quad (26)$$

Eq. (26) and the real and imaginary parts of Eq. (25) provide five non-linear simultaneous equations that are solved numerically to determine the required pulse timings for $0 \leqslant \Theta < 2\pi$. Numerical searches were implemented using Mupad [22] and required only a few seconds to find solutions, a Mupad procedure is available on request from the authors to calculate pulse times. The additional constraint that the sequence is of constant length for all values of Θ is also imposed.

For five π-pulse sequences, solutions to Eqs. (25) and (26) are readily calculated for $1 \leqslant N \leqslant 3.4$. In particular, sequences of a total length of one rotor period can be found with a scaling factor $1 \leqslant N < 2$. For scaling factors in the range $2 \leqslant N \leqslant 3.4$ the shortest sequences, which avoid pulse collisions and have π-pulses well separated in time, are $T = 4\tau_r$ in length. Using pulses spaced over four rotor periods may have the advantage that the effects due to finite pulse lengths will be less, particularly at higher spinning frequencies, than using pulses applied over a single rotor period. The pulse tim-

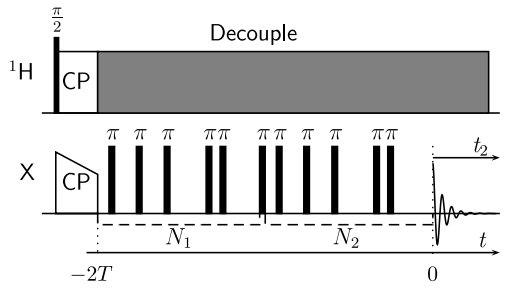

Fig. 2. Schematic form of the 11 pulse sequence constructed from two five-pulse units, separated by a π-pulse. The overall scaling factor is the sum of each five pulse unit: $N_{\text{Total}} = N_1 + N_2$.

ings as a function of Θ are plotted for $N = 3$ in Fig. 1B and $N = 2$ in Fig. 1C.

We have not found five π-pulse sequences that achieve larger scaling factors than $N = 3.4$. However, pulse sequences that do achieve higher scaling factors can be constructed by concatenating the basic five-pulse units, to achieve an overall scaling factor of equal to the sum of the scaling factor of each unit. This scheme is illustrated in Fig. 2. An additional π-pulse between adjacent five-pulse units is required so that coherences follows the same transfer pathway during each repetition of the five-pulse unit, otherwise the phase accumulation under the anisotropic components of chemical shift will be refocused by the repeated unit. This gives sequences of 11 and 17 π-pulses, with maximum scaling factors of 6.8 and 10.2. Larger scaling factors may, of course, be obtained using longer sequences, provided spectrometer stability can be ensured.

4. Phase cycling

Due to the use of several π-pulses at times synchronized with the sample spinning, the sequences are sensitive to experimental imperfections resulting from sample spinning instability, pulse miscalibration and field inhomogeneity. The effects of pulse imperfections are significantly reduced by phase cycling the X-channel cross-polarization pulse and each π-pulse. The required coherence transfer pathway for the five π-pulse 2D CSA-amplified PASS sequence is $0 \to +1 \to -1 \to +1 \to -1 \to +1 \to -1$. Conventional phase cycling increments the phase of each π-pulse independently in steps of $2\pi/3$; this uniquely selects the desired coherence pathway but requires $3^5 = 243$ phase cycle steps. This may be inconvenient for many samples, if recording so many scans is greater than is needed to achieve an acceptable signal-to-noise ratio, or impractical if a long pulse delay is required. When using the sequences of 11 or 17 π-pulses, phase cycles of 177,147 and 1.291×10^8 steps, respectively will certainly be impossible. The recently developed cogwheel phase cycling approach dramatically reduces the number of phase cycling steps required in these experiments. A phase cycle of only thirteen steps is needed to eliminate the effects of pulse miscalibration, field inhomogeneity, quadrature artefacts and zero-frequency artefacts for the five π-pulse sequence [23,24]. For the 11 π-pulse sequence the number of steps required is 25, and for the 17 π-pulse sequence 37 steps are needed to achieve the same level of coherence pathway selection and artefact elimination. Examples of explicit phase cycles that do not require cycling of the receiver or detector phase are given in Table 1.

Table 1
Cogwheel phase cycles, suitable for the 2D CSA-amplified PASS sequences, that do not require variation of the recorder or post digitizer phases ($\phi_{\text{rec}} + \phi_{\text{dig}} = 0$ in each case)

Number of π-pulses (n)	Cogwheel phase cycle	
	X-channel CP pulse	π-Pulses
5	$\phi_{\text{CP}} = \frac{-6*2\pi j}{13}$	$\phi_{q=\text{even}} = \frac{-6*2\pi j}{13}$, $\phi_{q=\text{odd}} = \frac{-5*2\pi j}{13}$
11	$\phi_{\text{CP}} = \frac{-12*2\pi j}{25}$	$\phi_{q=\text{even}} = \frac{-12*2\pi j}{25}$, $\phi_{q=\text{odd}} = \frac{-11*2\pi j}{25}$
17	$\phi_{\text{CP}} = \frac{-18*2\pi j}{37}$	$\phi_{q=\text{even}} = \frac{-18*2\pi j}{37}$, $\phi_{q=\text{odd}} = \frac{-17*2\pi j}{37}$

The index q identifies the π-pulse number within a sequence ($1 \leqslant q \leqslant n$); the required phase of the pulse only depends on whether q is even or odd. Variable j starts from zero and is increased by 1 following each scan of the experiment.

5. Experimental

^{32}P NMR experiments were performed on a Varian Infinityplus spectrometer, operating at 202.341 MHz for ^{31}P, using a 4 mm rotor. The pulse sequence used is illustrated in Fig. 1A with pulse timings achieving a scaling factor of $N = 3$, although the cross-polarization step and proton decoupling was omitted with ^{31}P transverse magnetization generated by a π/2-pulse. The ^{31}P π-pulse length was 12 μs and spinning frequency used was 5 kHz. The delay between scans was 600 s. The slow relaxation rate prevented even the proposed cogwheel phase cycling being implemented and instead fixed phases of the π-pulses of 0°, 330°, 60°, 330°, 0° were used, which have been reported to reduce the effects of pulse imperfections [20,11]. ^{13}C NMR experiments were implemented using a Bruker Avance spectrometer operating at 100.56 MHz for ^{13}C and 399.98 MHz for ^{1}H, using a 4 mm rotor. TPPM ^{1}H decoupling [25] was used with a field strength of 93 kHz, ^{13}C π-pulses were 5.7 μs and the contact time was 2 ms. A 17 π-pulse sequence was used, with 50 increments of Θ and cogwheel phase cycling of the pulses, to achieve a scaling factor of $N = 10.2$ at a spinning frequency of 5750 Hz. Sodium phosphate (Na_3PO_4) and fumaric acid monoethyl ester were obtained from Sigma–Aldrich and used without further purification.

6. Results and discussion

The MAS spectra of sodium phosphate spinning at 500 and 1666 Hz are shown in Figs. 3A and B. The effects of homonuclear dipolar coupling clearly dominate the spectrum spinning at 500 Hz, this suggests an application of this technique to samples for which slow spinning cannot be used to determine the chemical shift anisotropy from a simple one-dimensional experiment, even though there is only a single site. Faster spinning largely removes the effects of homonuclear dipole coupling, Fig. 3B, but leaves insufficient sidebands for quantitative CSA analysis.

As an experimental demonstration of the 2D CSA-amplified PASS sequence we have compared the integrated sideband intensities from the 1D MAS spectrum shown in Fig. 3B, which represents the lowest spinning rate at which ^{31}P homonuclear effects are largely absent. Although the number of sidebands is insufficient to determine the asymmetry parameter accurately, they are adequate to demonstrate the experiment, and the sample is convenient as only a single phosphorous site is present. These spinning sidebands are plotted as the solid line in Fig. 3D, and superimposed are the integrated sideband intensities obtained from the 2D CSA-amplified PASS spectrum with the same effective spinning frequency in Fig. 3C, shown as the dashed line and circles. The small residual sidebands in the direct dimension of the 2D CSA-amplified PASS spectrum spinning at 5000 Hz were added to the isotropic peak intensity to ensure accurate results. As expected, the integrated sideband intensities obtained from the 2D experiment are consistent with those obtained at the effective spinning frequency.

As a second example, the results for ^{13}C in fumaric acid monoethyl ester are given in Fig. 4, where a scaling factor of $N = 10.2$ is employed. Significant sideband intensities in the directly observed dimension were again added to the isotropic peak intensities to ensure accurate results. Numerical fits to the data were calculated using SIMPSON [26]; the simplex method was used to minimize the root mean square difference between the simulated and experimental data. For all six ^{13}C sites in the molecule good fits were obtained and values of the chemical shift anisotropy and asymmetry were determined, with the exception of the CH_3 site for which the asymmetry parameter was poorly defined.

A comparison with other experiments that can be used to extract the same information can be made. Table 2 shows the number of π-pulses used and length of the pulse sequences of 2D CSA-amplified PASS, CSA amplification, XCS and SPEED. Although the number of π-pulses in the 2D CSA-amplified PASS are applied over a larger number of rotor periods, the number of π-pulses required is similar to the XCS and SPEED experiments for similar CSA amplification factors. For

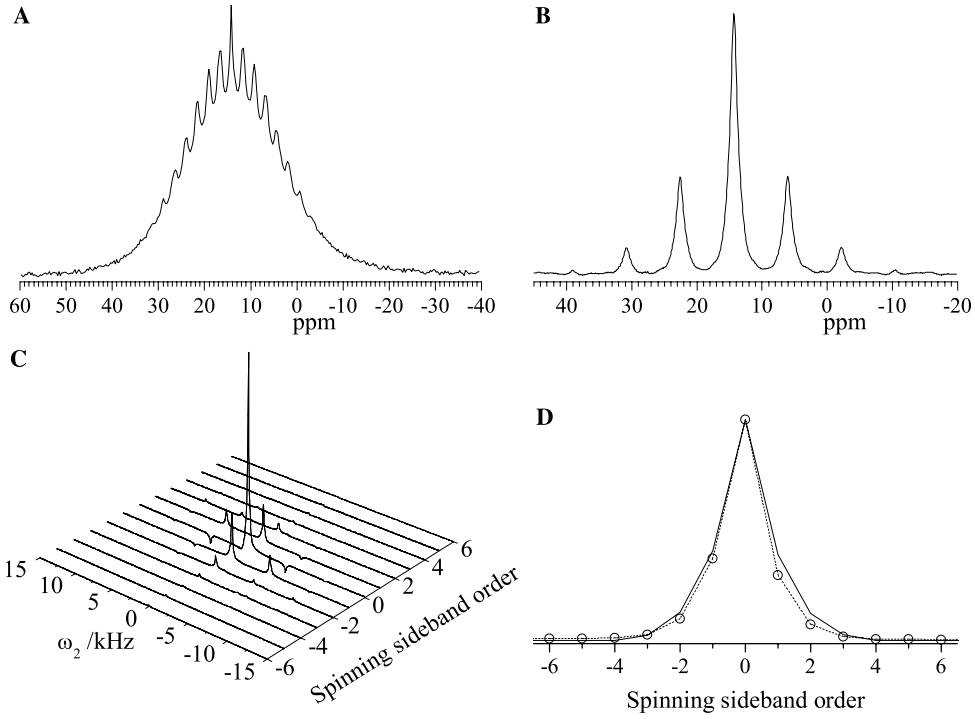

Fig. 3. Experimental ^{31}P NMR spectra of Na_3PO_4. (A) MAS spectrum spinning at 500 Hz. (B) MAS spectrum spinning at 1666 Hz. (C) 2D CSA-amplified PASS spectrum at a spinning frequency of 5000 Hz, using a 2D CSA-amplified PASS sequence with scaling factor $N = 3$. (D) Integrated sideband intensities of the 1D MAS spectrum spinning at 1666 Hz shown in (B) (solid line), and those derived from the 2D CSA-amplified PASS experiment shown in (C) (dashed line and open circles).

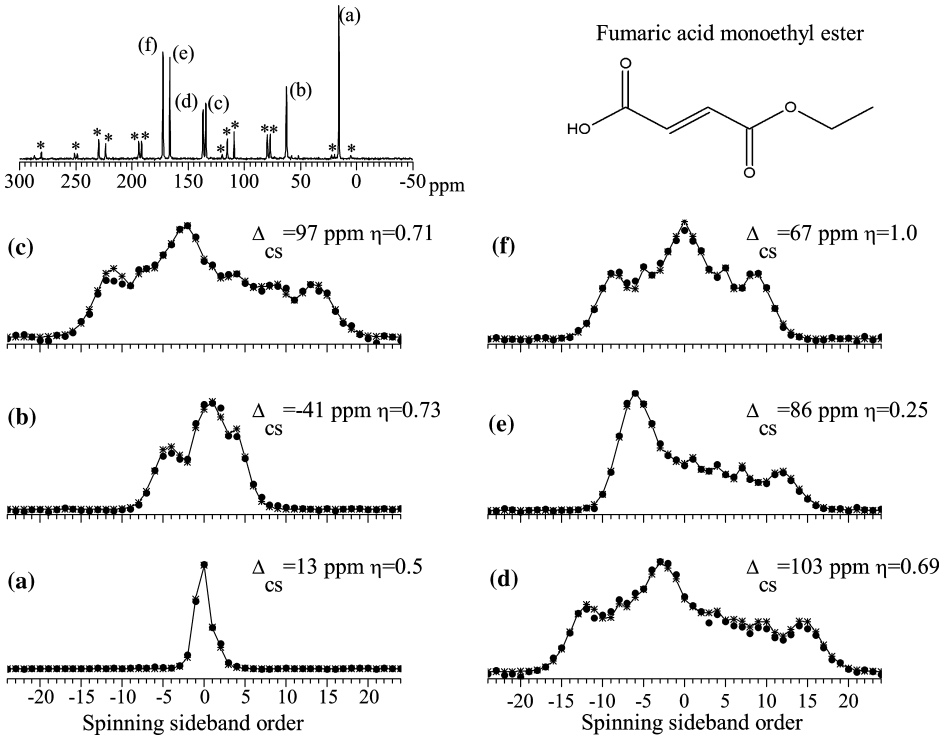

Fig. 4. Experimental ^{13}C NMR spectra of fumaric acid monoethyl ester at a spinning frequency of 5750 Hz. Asterisks mark spinning sidebands. (a–f) Experimental side band intensities determined using the 2D CSA-amplified PASS of this work (filled circles) for each isotropic peaks labelled in the 1D-spectrum, with an effective spinning frequency of 564 Hz (true spinning frequency of 5750 Hz and scaling factor $N = 10.2$). Simulated best fits are illustrated by the overlaid lines and asterisks, together with the CSA and asymmetry parameters used.

Table 2
Comparison of 2D CSA-amplified PASS sequences with CSA amplification [11,12], XCS [10] and SPEED [14]

N	2D CSA-amplified PASS		CSA amplification [11,12]		XCS [10]/SPEED [14]	
	π-pulses	Length[a]/τ_r	π-pulses	Length[a]/τ_r	π-pulses	Length[a]/τ_r
2	5	4	$8(+2\frac{\pi}{2}-\text{pulses})$	5	3	2
3	5	4	$8(+2\frac{\pi}{2}-\text{pulses})$	5	5	3
4	11	5	$8(+2\frac{\pi}{2}-\text{pulses})$	5	7	4
5	11	8	$8(+2\frac{\pi}{2}-\text{pulses})$	5	9	5
6	11	8	$8(+2\frac{\pi}{2}-\text{pulses})$	5	11	6
7	17	9	$10(+2\frac{\pi}{2}-\text{pulses})$	7	13	7
8	17	12	$10(+2\frac{\pi}{2}-\text{pulses})$	7	15	8
9	17	12	$14(+2\frac{\pi}{2}-\text{pulses})$	9	17	9
10	17	12	$14(+2\frac{\pi}{2}-\text{pulses})$	9	19	10
11	23	16	$14(+2\frac{\pi}{2}-\text{pulses})$	9	21	11
12	23	16	$14(+2\frac{\pi}{2}-\text{pulses})$	9	23	12

[a] Duration of the pulse sequence from the end of the cross-polarization pulse, to the start of signal detection.

amplication factors of 7 and above, the 2D CSA-amplified PASS experiment requires 5 or more additional pulses to the CSA amplification method and delivered over a longer time period ($2\tau_r$ longer for an amplification factor of 7; $7\tau_r$ for an amplification factor of 12). The more pulses applied and the longer the duration of the sequence, the lower the potential sensitivity of the experiment. Thus it may be that for higher chemical shift amplification factors, the extra sensitivity gained in the 2D CSA-amplified PASS experiment by the absence of a storage period is lost when compared with the chemical shift amplification method. To a certain extent, such considerations will be both spectrometer and sample dependent and there is no clear choice in general until very large amplification factors are reached. Further advantages of the 2D CSA-amplified PASS experiment are the fixed length of the pulse sequence for all Θ, which prevents phasing effects that can result from differing degrees of transverse relaxation in signals acquired for different t_1 increments and the fact that

phase cycling using a practical number of steps, can be implemented to select a single coherence pathway, which compensates for the effects of pulse imperfections, field inhomogeneity and other artefacts. In practice it may be possible to use cogwheel phase cycling in the other experiments discussed, to enable a reduction in the number of phase cycles.

7. Conclusion

An experiment to measure chemical shift tensors that are small compared with the spinning frequency has been demonstrated, and the method for the construction of the required pulse sequences to achieve a wide range of scaling factors, N, has been detailed. The experiment has been successfully demonstrated with a scaling factor of $N = 10.2$ for ^{13}C in fumaric acid monoethyl ester, spinning sideband patterns for all six ^{13}C sites in this compound were shown to be accurately produced by the experiment through simulations.

Acknowledgments

We are grateful to the Royal Society for the award of a Dorothy Hodgkin Research Fellowship (S.E.A.) and the Engineering and Physical Sciences Research Council for a studentship (R.M.O.).

Appendix A. Supplementary data

Supplementary data associated with this article can be found, in the online version, at doi:10.1016/j.jmr.2005.03.001.

References

[1] M.M. Maricq, J. Waugh, NMR in rotating solids, J. Chem. Phys. 70 (1979) 3300–3316.
[2] J. Herzfeld, A.E. Berger, Sideband intensities in NMR spectra of samples spinning at the magic angle, J. Chem. Phys. 73 (1980) 6021–6031.
[3] P. Hodgkinson, L. Emsley, The reliability of the determination of tensor parameters by solid-state nuclear magnetic resonance, J. Chem. Phys. 107 (1997) 4808–4816.
[4] L. Frydman, G. Chingas, Y. Lee, P. Grandinetti, M. Eastman, G. Barrall, A. Pines, Variable-angle correlation spectroscopy in solid-state nuclear magnetic resonance, J. Chem. Phys. 97 (1992) 4800–4808.
[5] Z. Gan, High-resolution chemical shift and chemical shift anisotropy correlation in soluds using slow magic angle spinning, J. Am. Chem. Soc. 114 (1992) 8307–8310.
[6] R. Tycko, G. Dabbagh, P.A. Mirau, Determination of chemical-shift-anisotropy lineshapes in a two-dimensional magic-angle-spinning NMR experiment, J. Magn. Reson. 85 (1989) 265–274.
[7] S. Liu, J. Mao, K. Schmidt-Rohr, A robust technique for two-dimensional separation of undistorted chemical-shift anisotropy powder patterns in magic-angle-spinning NMR, J. Magn. Reson. 155 (2002) 15–28.
[8] O.N. Antzutkin, S.C. Shekar, M.H. Levitt, Two-dimensional sideband separation in magic-angle-spinning NMR, J. Magn. Reson. 115 (1995) 7–19.
[9] A.C. Kolbert, D.P. Raleigh, M.H. Levitt, R.G. Griffin, Two-dimensional spin-echo nuclear magnetic resonance in rotating solids, J. Chem. Phys. 90 (1989) 679–689.
[10] T. Gullion, Extended chemical-shift modulation, J. Magn. Reson. 85 (1989) 614–619.
[11] C. Crockford, H. Geen, J.J. Titman, Two-dimensional MAS-NMR spectra which correlate fast and slow magic-angle spinning sideband patterns, Chem. Phys. Lett. 344 (2001) 367–373.
[12] L. Shao, C. Crockford, H. Geen, G. Grasso, J.J. Titman, Chemical shift anisotropy amplification, J. Magn. Reson. 167 (2004) 75–86.
[13] B. Eléna, S. Hediger, L. Emsley, Correlation of fast and slow chemical shift spinning sideband patterns under fast magic-angle spinning, J. Magn. Reson. 160 (2003) 40–46.
[14] M. Strohmeier, D.M. Grant, A new sensitive isotropic-anisotropic separation experiment—SPEED MAS, J. Magn. Reson. 168 (2004) 296–307.
[15] S. De Lacroix, J.J. Titman, A. Hagemeyer, H. Spiess, Increased resolution in MAS NMR spectra by two-dimensional separation of sidebands by order, J. Magn. Reson. 97 (1992) 435–443.
[16] S. Hartmann, E. Hahn, Nuclear double resonance in the rotating frame, Phys. Rev. 128 (1962) 2042–2053.
[17] C. Crockford, New methodologies in solid-state NMR, Ph.D. Thesis, University of Nottingham, 2002.
[18] G. Metz, X. Wu, S. Smith, Ramped-amplitude cross polarization in magic-angle-spinning NMR, J. Magn. Reson. Ser. A 110 (1994) 219–227.
[19] M.H. Levitt, Why do spinning sidebands have the same phase?, J. Magn. Reson. 82 (1988) 427–433.
[20] O. Antzutkin, Z. Song, X. Feng, M. Levitt, Suppression of sidebands in magic-angle-spinning nuclear magnetic resonance: general principles and analytical solutions, J. Chem. Phys. 100 (1994) 130–140.
[21] O. Antzutkin, Sideband manipulation in magic-angle-spinning nuclear magnetic resonance, Prog. Nucl. Magn. Res. Spectrosc. 35 (1999) 203–266.
[22] SciFace Software GmbH & Co.KG, Mupad Computer Algebra System, Paderborn.
[23] M.H. Levitt, C.E. Hughes, P.K. Madhu, Cogwheel phase cycling, J. Magn. Reson. 155 (2002) 300–306.
[24] N. Ivchenko, C.E. Hughes, M.H. Levitt, Application of cogwheel phase cycling to sideband manipulation experiments in solid-state NMR, J. Magn. Reson. 164 (2003) 286–293.
[25] A.E. Bennett, C. Rienstra, M. Auger, K.V. Lakshmi, R. Griffin, Heteronuclear decoupling in rotating solids, J. Chem. Phys. 103 (1995) 6951–6958.
[26] M. Bak, J. Rasmussen, N. Nielsen, SIMPSON: a general simulation program for solid-state NMR spectroscopy, J. Magn. Reson. 147 (2000) 296–330.